The Effect Of Bird Strike On The Performance Of A NACA 2412

Arief Hadiyanto, Dominicus Danardono Dwi Prija Tjahjana*, and Eko Prasetya Budiana

Department of Mechanical Engineering, Faculty of Engineering, Universitas Sebelas Maret, Jl. Ir. Sutami 36A, Surakarta 57126, Indonesia

Corresponding author. E-mail: ddanardono@staff.uns.ac.id

Received: Feb. 02, 2023; Accepted: Jun. 30, 2023

Damage to the leading edge in the form of dents due to bird strikes causes a decrease in the airfoil performance. Therefore, the current study provides a numerical analysis of the aerodynamic characteristics of the original NACA 2412 airfoil and the dent airfoil with depth variation. Several airfoils were compared for their lift and drag coefficients at an angle of attack of 0° to 6°. The free air flow velocity was kept constant at the Reynolds number of 3.1×10^6. Computational fluid dynamics (CFD) was used, employing the k-ω SST turbulence model to obtain accurate calculations on the airfoil surface. The simulation results revealed that the dented NACA 2412 airfoil lift coefficient (C_L) decreased while the drag coefficient (C_D) increased, where the value varied with changes in the angle of attack and depth of the dent.

Keywords: Bird strike, Lift, Drag, CFD

http://dx.doi.org/10.6180/jase.202404_27(4).0004

1. Introduction

Bird strikes are becoming a concerned issue in the aviation industry. The first bird strike occurred on September 7, 1905, in Dayton, Ohio, USA, when Orville Wright's plane hit a bird [1]. On April 3, 1912, the first fatal accident resulting from a bird strike occurred, causing the death of Calbraith Rodgers [2]. ICAO (International Civil Aviation Organization) as the international aviation authority on May 12, 2017, reported that in a period of eight years (2008-2015), 97,751 wildlife strikes occurred [3]. As a consequence, ICAO and other world aviation authorities, such as the Federal Aviation Authorization (FAA) and Civil Aviation Authority (CAA), require a guarantee of safety in the world of aviation in the form of a certificate of airworthiness [4].

The term bird strike can be defined as a collision between a bird and an airplane which, in most cases, affects the aerodynamic performance of the aircraft. The most vulnerable aircraft structure to a bird strike is at the front face, such as the windshield, radome, engines, propeller, and wing leading edge [5–7]. Among the parts of the aircraft that often experience bird strikes, the wing's leading edge is one of the most frequently experienced parts, accounting for 31% of occurrences [8]. Bird strike on the wing structure causes changes in the shape of the wing profile [4], which in most of the existing literature only provides their impact on the wing's deformation. The current study focused on the effect of bird strikes on the aerodynamic performance to provide a different sight of bird strike impact on the wings structure. The depth and width of dents caused by bird strikes are of concern in the research. Therefore, to support our research, the review of the bird strike's effect on wing structure, physical phenomena that occur due to the bird strike, the problem statement, and the objective will be explained hereafter.

Much research has been done to determine the effect of bird strikes on the wing's leading edge. The results of previous studies, both in computer modeling and experiments, show that the damage caused by bird strike causes severe damage to the leading edge [9–13]. Riccio et al. [9] used

numerical approaches to model the crack in the composite structure due to the bird strike, including matrix cracking and bird deformation. The damage mechanism starts from the matrix transaction, leading to stiffness reduction. The wing structure's deformation prediction and damage behavior were also studied by Liu et al.[10]. Under the numerical study, they found that the displacement of the impact region because of tensile stretching was the main reason for the leading-edge skin material failure. Long et al. [11] characterized the failure under the dynamic response of the composite structure due to the bird impact. They proposed that material failure subjected to the bird strike can be reduced using a laminated structure with stacking sequences. The configuration can reduce the shear and bending tensions, thus enhancing the resistance ability toward the bird strike. May et al. [12] also proposed improvements in bird strike resistance. Fibered composites in the form of CFRP were employed for the material selection to be analyzed and modeled using a leading-edge morphing design. They found that CFRP skin was not strong enough to avoid the leading-edge damage. Therefore, they improved the model by adding bird strike protection using a bird splitter. Even then, the bird strike might come from a different direction. Tatlier et al. [13] performed numerical studies on the impact of the different orientations of the bird strike. They found that the changes in the bird strike direction produced a negligible effect on the deformation.

From the above literature, the research on the bird strike is mostly concerned with the deformation of the wing structure. However, how they would impact the aerodynamic performance still required further investigation. Research on the aerodynamic performance of wings that experience bird strikes and how the air flow in the leading edge area of the wing deforms due to bird strikes is still very limited. Only Tatlier and Baran [4] have conducted research on the aerodynamic characteristics of a 3-dimensional NACA 9417 airfoil that was deformed by a bird strike. It is found that there are changes in flow behavior in the deformed region affect the aerodynamic performance of the wing. In the meantime, Wang et al. [14] examine the steady and dynamic stall characteristics of the wind turbine blades that damage to the leading edge of wind turbine blades due to continuous impact with raindrops, insects, or solid particles during its operation. The turbine blade was modeled in two dimensional S809 airfoil, and the damage of the leading edge is assumed to be semi-rectangular. Current research provides a numerical study of the depth of the dent caused by bird strikes to analyze their effect on the aerodynamic performance of the airfoil.

The NACA 2412 airfoil is considered in this study because this airfoil is used on single-engine aircraft, such as the Cessna 152, Cessna 172, and Cessna 182 [15]. The wings are assumed to have defects in the form of dents in the leading-edge area due to bird strikes. Thus, it is estimated that there will be changes in the aerodynamic performance of the wing. Based on that, the idea arose to compare the airflow characteristics on the NACA 2412 airfoil wings before and after experiencing a bird strike employing a numerical method, i.e., CFD (Computational Fluid Dynamics) modeling. CFD modeling was chosen since it was deemed more effective and efficient, and the CFD results agreed with wind tunnel experiments' experimental results [16–19]. The research provides knowledge about the effect of bird strikes on wing aerodynamic performance, emphasizing the influence of the depth of the defect.

2. Theory and formula

2.1. Conceptual Design

This study compared the aerodynamic performance of NACA 2412 airfoil wings by analyzing changes in airflow characteristics on the wings before and after experiencing a bird strike. The shape and size of the dent referred to the reference [20], which existed around 285 mm with a depth ranging from 40-50 mm [20]. The condition of the aircraft was assumed when flying level flight at a speed of 90 knots (46.3 m/s).

Numerical simulation tests utilizing ANSYS Student 2022R1 software were carried out to determine changes in wing airflow characteristics. This software has limitations for computational analysis since it can only analyze the meshing results with a maximum of 512,000 cells (elements) or nodes [21].

2.2. Governing Equation

The investigation was conducted under 2D modeling. The consideration of aerodynamic calculations assumed that the flow was steady and incompressible. The analyses applied the law of conservation in physics, namely the law of conservation of mass, conservation of momentum, and energy conservation. Nevertheless, since it did not involve heat transfer, the law of conservation of energy was not used in this calculation.

Due to the continuity equation for 2-D flow with cartesian coordinates x and y, the equation for the law of conservation of mass is reduced to the following:

$$\frac{\partial u}{\partial x} + \frac{\partial v}{\partial y} = 0 \tag{1}$$

The equation for the law of conservation is the Navier Stokes momentum equation for 2-D flow with cartesian

coordinates x, y, written as follows:

$$x : \rho\left(u\frac{\partial u}{\partial x}+v\frac{\partial u}{\partial y}\right)=-\frac{\partial p}{\partial x}+\mu\left(\frac{\partial^2 u}{\partial x^2}+\frac{\partial^2 u}{\partial y^2}\right) \quad (2)$$

$$y : \rho\left(u\frac{\partial v}{\partial x}+v\frac{\partial v}{\partial y}\right)=-\frac{\partial p}{\partial y}+\mu\left(\frac{\partial^2 v}{\partial x^2}+\frac{\partial^2 v}{\partial y^2}\right) \quad (3)$$

Additionally, k-ω SST was used as the turbulence equation, as follows:

$$\frac{\partial_{(\rho k)}}{\partial t}+\frac{\partial_{(\rho u_j k)}}{\partial x_j}=\rho P-\beta^*\rho\omega k+\frac{\partial}{\partial x_j}\left[\left(\mu+\sigma_k\frac{\rho k}{\omega}\right)\frac{\partial_k}{\partial x_j}\right] \quad (4)$$

$$\frac{\partial_{(\rho\omega)}}{\partial t}+\frac{\partial_{(\rho u_j\omega)}}{\partial x_j}=\frac{v}{u_t}P-\beta\rho\omega^2+\frac{\partial}{\partial x_j}\left[(\mu+\sigma_\omega\mu_t)\frac{\partial_\omega}{\partial x_j}\right]+2(1-F_1)\sigma_{\omega^2}\frac{1}{\omega}\frac{\partial_k}{\partial x_j}\frac{\partial_\omega}{\partial x_j} \quad (5)$$

3. Experimental setup

3.1. Wing Model

The NACA 2412 airfoil model was made in geometry before and after experiencing a bird strike. NACA 2412 airfoil data plotted results from the website www.airfoiltools.com, with a chord length (c) of 1000 mm. The basic specifications for the NACA 2412 airfoil model are displayed in Table 1.

Table 1. Specifications for the Original NACA 2412 Airfoil Model.

No	Description	Dimension
1.	Type airfoil	NACA 2412
2.	Chord length	1000 mm
3.	Max camber (2% chord length)	20 mm
4.	Max camber position (40% chord length)	400 mm
5.	Thickness (12% chord length)	120 mm

On the NACA 2412 airfoil model, after experiencing a bird strike, the dented area was located on the leading edge, as illustrated in Fig. 1, where x is the depth of the dent, and h is the height of the dent. There are four types of dented NACA 2412 airfoil models. The specifications for the dented NACA 2412 airfoil model are shown in Table 2.

3.2. Computational Domain Modeling

The computational domain modeling consisted of a solid domain in the form of a NACA 2412 airfoil and a fluid domain in the form of an enclosure. The enclosure used was C domain. The front of C domain had a semicircular shape, with a radius of 15c, and the back was a rectangle, with a length of 30c [14, 22]. To get better meshing, the face split technique is used.

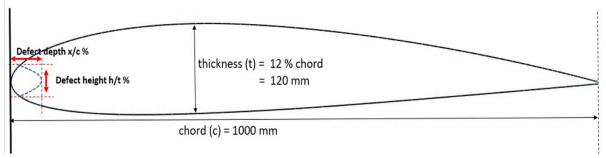

Fig. 1. Assumed location of dent depth and height.

3.3. Meshing

The initial step of meshing was with the default mesh settings. To improve the quality of the mesh, edge sizing and face meshing techniques were employed. In the computing domain, inlets were defined on the enclosure faces of the front, bottom, and top airfoils, outlets were defined on the enclosure faces of the rear airfoil, and objects were defined on the 2412 model airfoil.

In addition, the meshing process produced 377,505 nodes and 376,002 elements. The resulting mesh quality had an average skewness of 5.9375×10^{-2} and an average orthogonal quality of 0.9817. The meshing results can be seen in Fig. 2. Since it had a skewness close to 0 and orthogonal quality close to 1 (mesh quality reference), the resulting mesh could be considered good quality.

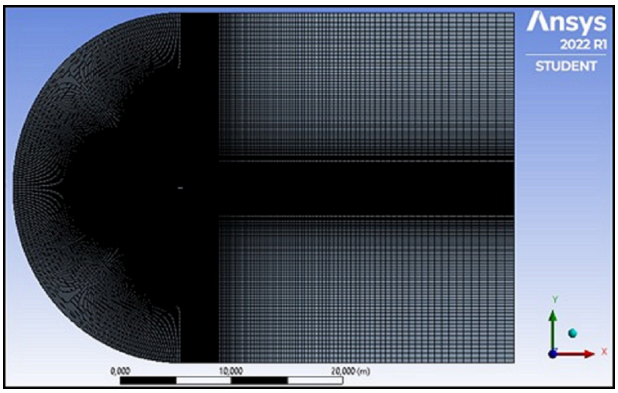

Fig. 2. NACA 2412 airfoil 2D meshing results computing process.

The NACA 2412 airfoil was modeled in two dimensions (2D). This model was chosen because the comparison of the values of the lift coefficient and the drag coefficient of 2D simulation data with 3D experiments has a similar trend [23]. Time is assumed to be steady, the condition where the fluid properties at a point in the system do not change over time.

ANSYS provides a variety of turbulence simulation models [24]. The k-ω SST model was used as a viscous model to obtain accurate calculations on walls, and the results of simulation calculations were close to those of

Table 2. Types of dented NACA 2412 airfoil models.

No	Dented Airfoil Model	Dent thickness (h/t %)	Dent depth (x/c %)
1.	Airfoil Dented at 35 mm	34.2 % (h = 41 mm)	3.5 % (x = 35 mm)
2.	Airfoil Dented at 40 mm	34.2 % (h = 41 mm)	4 % (x = 40 mm)
3.	Airfoil Dented at 45 mm	34.2 % (h = 41 mm)	4.5 % (x = 45 mm)
4.	Airfoil Dented at 50 mm	34.2 % (h = 41 mm)	5 % (x = 50 mm)

experimental calculations [16, 19]. In addition, this model could predict the accuracy of flows well, with adverse pressure gradients and strong separations [25]. The boundary conditions in the research domain are as presented in Table 3, with an angle of attack between 0°-6°.

Table 3. Boundary conditions.

No	Boundary Area	Boundary Conditions	Information
1.	Inlet	Velocity Inlet	46.3 m/s
2.	Outlet	Pressure Outlet	0 Pa gage pressure
3.	Wall	Airfoil	No slip

3.4. Validation

Validation aimed to confirm that the simulation carried out described the actual situation. Validation was performed by comparing C_L and C_D values on 2D NACA 2412 airfoil from XFoil software data as comparison data, while simulation data were taken utilizing ANSYS Fluent software.Fig. 3(a) and (b) reveal the validation results. The graph of the simulation results depicts that the simulation results had relatively good accuracy. The average error value of this comparison is 5.37% for C_L errors and 8.60% for C_D errors. It can be concluded from the analysis that the two graphs had a similar trendline and sometimes coincided with the C_L and C_D graphs from the ANSYS Fluent simulation with XFoil.

4. Results and discussion

The simulation data comprised several data, presented in graphs and contours. Fig. 4(a), (b), and (c) are graphs of C_L, C_D, and C_L/C_D comparison results. These data showed differences in aerodynamic performance in the various airfoils being compared. In the meantime, the comparison of the average value of C_L, C_D, and C_L/C_D on the original NACA 2412 airfoil and several types of dented airfoils model are shown in Table 4.

Based on Fig. 4(a), the simulation results on the original NACA 2412 airfoil and several types of dented airfoils suggest that the C_L values showed a similar trend line and tended to coincide for several types of dented airfoils, especially at low angles of attack (0°-3°). The graph illustrates

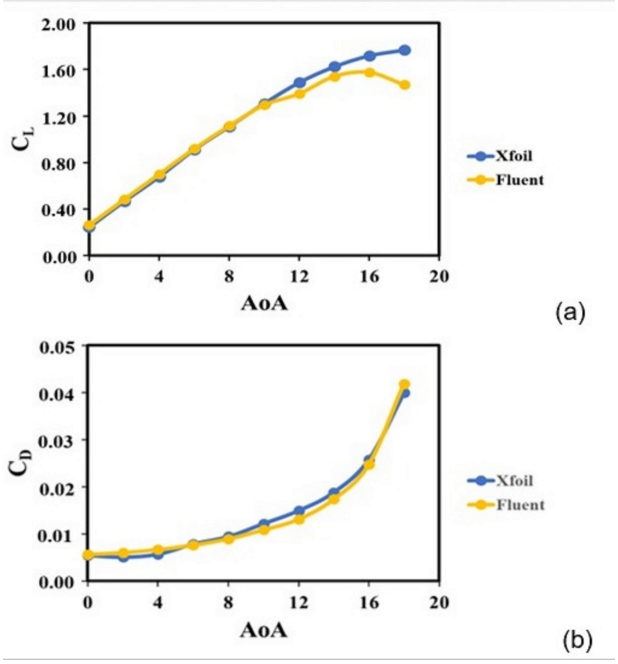

Fig. 3. Graph of comparison of C_L (a) and C_D (b), of the original NACA 2412 airfoil simulation results with XFoil data.

that the C_L value increased with the increasing angle of attack. In addition, the C_L average value on all types of dented airfoils for all angles of attack had a smaller value than the original airfoil. These results are in accordance with the results of research conducted by Tatlier and Baran [4] and Wang et al. [14].

The average C_L value of the original airfoil is 0.5901. While the highest average value of C_L dented airfoil is 0.5649 at a depth of 35 mm, and the lowest average value of C_L dented airfoil is 0.5177 at a depth of 50 mm. The percentage decrease in the average C_L value of the original airfoil to the smallest C_L airfoil average value (airfoil dent 50 mm) is 12.28%. Dent in the airfoil causes a reduction in the chord length of the airfoil. In addition, the airflow that should flow smoothly and accelerate to the shoulder becomes disturbed because the stagnation area at the leading edge expands. Flow disturbance occurs both flowing to the upper surface and the lower surface of the airfoil, causing bubble flow separation [14].

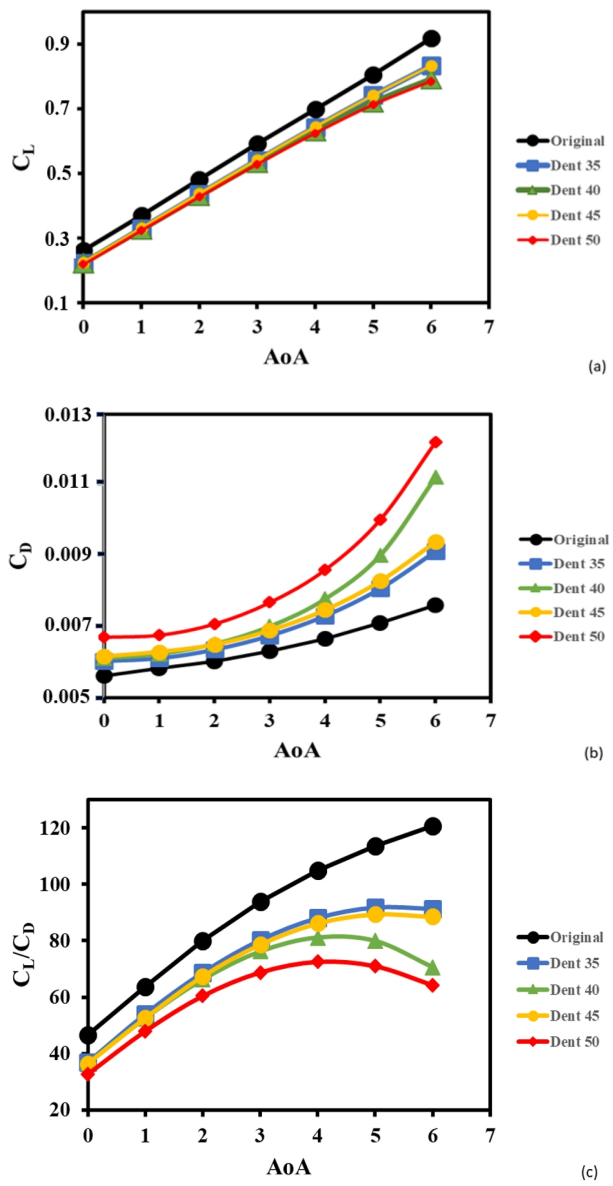

Fig. 4. Graph of simulation results comparison of C_L (a), C_D (b), and C_L/C_D (c), between the original NACA 2412 airfoil and dented airfoil at 35 mm, 40 mm, 45 mm, and 50 mm.

From the graph, it can also be seen that the increase in the dent's depth did not give a trendline for a linear decrease in the C_L value of the dent in the airfoil, but oscillations occurred. The C_L value on the dented airfoil with a depth of 35 mm and 45 mm had the same trendline. Likewise, C_L values on dented airfoils with a depth of 40 mm and 50 mm had the same trendline. However, in the dent airfoil with a depth of 40 mm and 50 mm, the C_L value was smaller than 45 mm.

Fig. 4(b) shows that the simulated C_D curve revealed an increasing value as the angle of attack increased. Also, in line with the results of Tatlier and Baran [4] and Wang et al. [14], the C_D value of the dented airfoils was greater than the original airfoil. The average value of the original C_D airfoil is 0.0064. While the highest average value of dent airfoil C_D was 0.0084 at a dent depth of 50 mm, and the lowest average value of dent airfoil C_D was 0.0071 at a dent depth of 35 mm. The average C_D value increased by 23.63% for the highest C_D airfoil average value (airfoil dent 50 mm) compared to the original airfoil.

However, there was a phenomenon where the increased depth of the dent did not give a linear trendline increase in the C_D value on the dent airfoil, but oscillations occurred. In addition, the graphs on the dented airfoil with a depth of 35 mm and 45 mm tended to coincide and had very similar trendlines. Moreover, the charts on the dented airfoil with a depth of 40 mm and 50 mm had very similar trendlines and did not coincide. Meanwhile, the stagnation area on the dented airfoil was more extensive than the original airfoil. It was due to trapped pressure on the dented profile in the leading-edge area. In other words, the larger the stagnation area, the greater the resulting C_D.

From Fig. 4(c), the aerodynamic efficiency of the distorted wing profile, measured by the lift to drag ratio (C_L/C_D), decreases notably when compared to the wing profile that has not been deformed. This is because, in deformed airfoils, there is an increase in C_D value followed by a decrease in C_L value. The same thing happened in previous studies [4, 14]. Besides, there was a phenomenon where increasing the dent depth did not give a linear trendline of decreasing C_L/C_D values on the dent airfoil, but oscillations occurred. Further, the C_L/C_D graphs on dented airfoils with a depth of 35 mm and 45 mm tended to coincide and had very similar trendlines. Meanwhile, C_L/C_D graphs on dented airfoils with 40 mm and 50 mm depth had very similar trendlines and did not coincide. From all the graphs, the original airfoil had a greater value than the dented airfoil. The average value of the original C_L/C_D airfoil is 89.0968. While the highest average value of dent airfoil C_L/C_D was 72.9846 at a dent depth of 35 mm, and the lowest average value of dent airfoil C_L/C_D was 59.7004 at a dent depth of 50 mm. In addition, of all the dented airfoils compared, the dented airfoil with a depth of 50 mm had the worst aerodynamic performance. The percentage decrease in the average C_L/C_D value of the original airfoil to the smallest C_L/C_D airfoil average value (airfoil dent 50 mm) is 32.99%.

Further, Fig. 5 illustrates the pressure coefficient (Cp) along the wing surface. The graph compares the pressure

Table 4. Average value of C_L, C_D, and C_L/C_D on original NACA 2412 airfoil and dented at 35 mm, 40 mm, 45 mm, and 50 mm (0° - 6° AoA).

No	Airfoil	Average C_L	Average C_D	Average C_L/C_D
1	NACA 2412 Original	0.5901	0.0064	89.0968
2	NACA 2412 Dent 35	0.5649	0.0071	72.9846
3	NACA 2412 Dent 40	0.5232	0.0077	66.1885
4	NACA 2412 Dent 45	0.5366	0.0073	71.3538
5	NACA 2412 Dent 50	0.5177	0.0084	59.7004

coefficient between the original airfoil and several dented airfoils at an angle of attack of 6°. The graphs of all airfoils showed the same trend. However, there were differences in the location of the stagnation point. The stagnation point on all dented airfoils was behind the stagnation point of the original airfoil due to deformation effects in the form of dents on the leading edge of all dented airfoils. The deformed airfoils also show a shrinkage of the area between the Cp graph lines compared to the original airfoil Cp graph. This shrinkage indicates a decrease in the C_L value of the 2-dimensional airfoil [14].

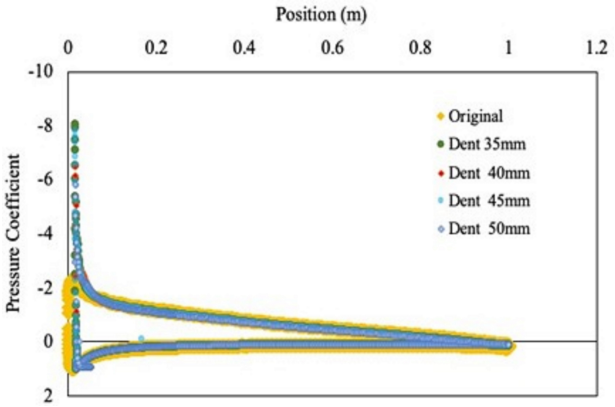

Fig. 5. Graph of Pressure Coefficient of Original NACA 2412 Airfoil and Dented at 35 mm, 40 mm, 45 mm, and 50 mm at AoA of 6°.

Then, Fig. 6 demonstrates the pressure coefficient contour on the original airfoil and dented airfoil with the smallest aerodynamic performance on a 50 mm dent at an angle of attack of 6°. From this figure, the stagnation area on the dented airfoil was larger than that of the original airfoil. It was due to trapped pressure on the dented profile in the leading-edge area. In other words, the larger the stagnation area, the greater the resulting C_D.

Then, Fig. 7 presents the velocity contour on the original airfoil and dented airfoil with the smallest aerodynamic performance on a 50 mm dent at an angle of attack of 6o. An analysis was then carried out on the leading edge, trailing edge, and the entire airfoil surface. The flow velocity on the leading edge runs smoothly on the original airfoil. Meanwhile, in a dented airfoil, the fluid flow was trapped in the dented profile in the leading-edge area so that the velocity became zero. At the top of the original airfoil, the fluid flow velocity, in general, was greater than that of the dented airfoil. It resulted in the C_L value on the original airfoil being greater than the dented airfoil. Besides, on the trailing edge, the flow separation on the dented airfoil occurred earlier.

Next, Fig. 8 shows the flow distribution along the airfoil surface. In both airfoils, the fluid flow tended to adhere along the airfoil. However, the fluid flow was interrupted when it passed through the leading edge of the dented airfoil. The fluid flow was trapped in the dented area and caused a decrease in flow velocity. After passing the leading edge, the flow velocity on the dented airfoil was higher than the original airfoil. However, a large pressure gradient created a tendency for separation bubbles to form in that area. It resulted in the C_L value on the original airfoil being greater than the dented airfoil. In addition, on the trailing edge, the fluid flow tended to move away from the surface, resulting in earlier separation of the flow in the dented airfoil so that the resulting C_D was greater.

5. Conclusion

A comparative numerical study of the aerodynamic performance of the NACA 2412 airfoil due to a bird strike in the form of dents on the leading edge is discussed in this paper. Calculations were performed on the Reynolds number of 3.1 $\times$ 106 with the k-ω SST turbulence model. Validation was then performed by comparing the data from the Xfoil.

CFD analysis reveals that the aerodynamic performance is affected by the dents on the leading edge. In this case, the dented airfoil has a smaller C_L value and a larger C_D value than the original airfoil at all angles of attack. Further analysis reveals that the dents on the leading edge cause the lift to drag ratio to decrease. This comparison interprets that bird strikes reduce aerodynamic performance.

In a dented airfoil, the stagnation area was larger than that of the original airfoil. Fluid flow was interrupted as it passed over the leading edge, causing a decrease in flow

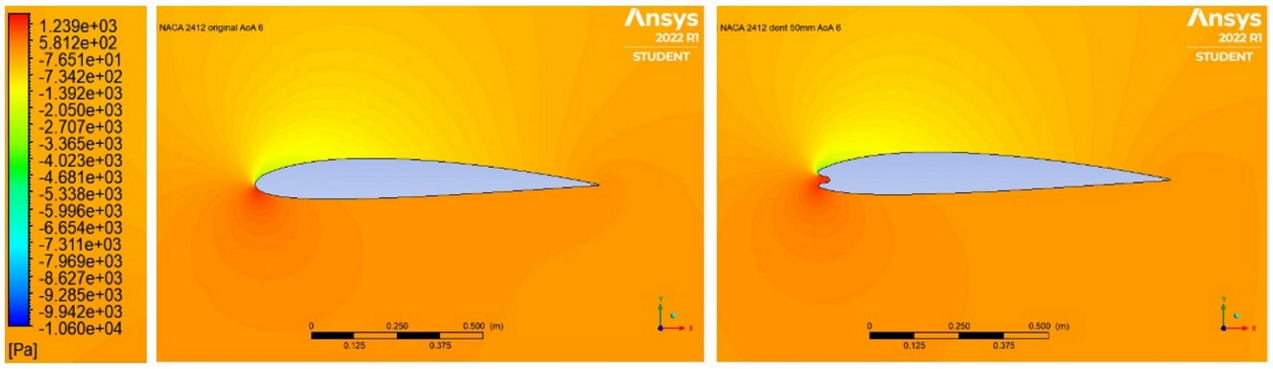

Fig. 6. Pressure Coefficient Contour of Original Airfoil vs. Airfoil Dented at 50 mm at AoA of 6°.

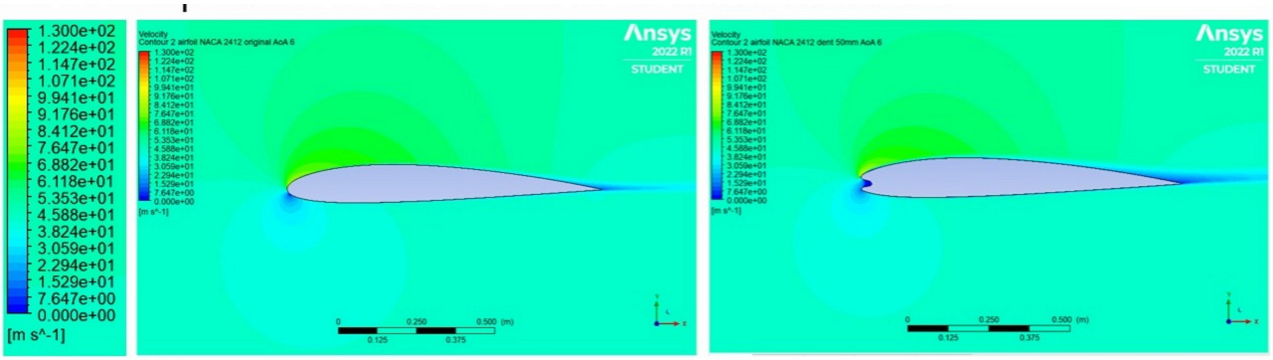

Fig. 7. Velocity Contour of Original Airfoil vs. Dented Airfoil on 50 mm at AoA of 6°.

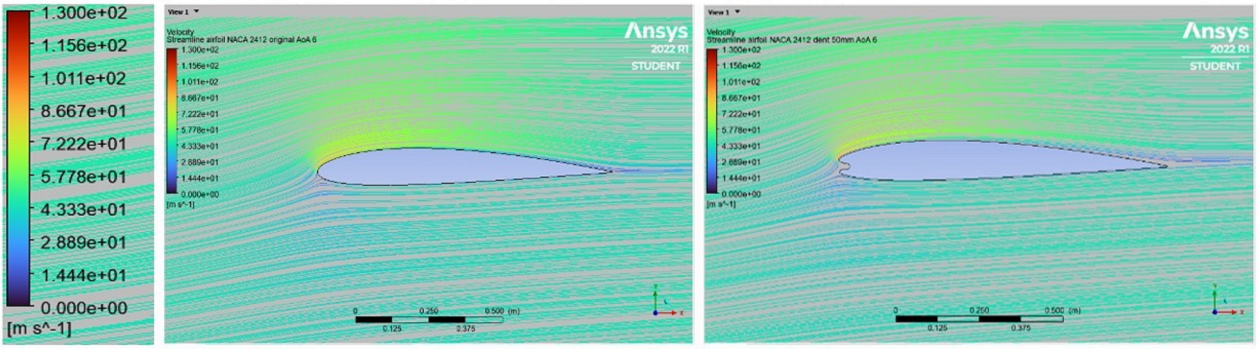

Fig. 8. Velocity Streamlines of Original Airfoil vs. Dented Airfoil on 50 mm at AoA of 6°.

velocity along the airfoil. In addition, the dented airfoil stagnation point was behind the original airfoil stagnation point due to deformation effects in the form of dents on the leading edge. This affects the increase in C_D value.

Further analysis reveals that the deformed airfoils also show a shrinkage of the area between the Cp graph lines compared to the original airfoil Cp graph. This shrinkage indicates a decrease in the C_L value.

The 2D modeling of airfoil NACA 2412 airfoil was done in this study. In order to make the research data closer to the actual condition, further research needs to be carried out in a 3D model of the NACA 2412 airfoil. In addition, to add insight, it is necessary to conduct research on the effect of dent location variations on aerodynamic performance.

References

[1] R. A. Dolbeer, (2013) *"The history of wildlife strikes and management at airports"* **Wildlife in Airport Environments: Preventing Animal-Aircraft Collisions Through Science-Based Management**: 1–7.

[2] E. C. Cleary and R. A. Dolbeer, (2005) *"Wildlife Hazard Management at Airports"* **Federal Aviation Administration**: 362.

[3] 2. .-. 2. W. S. A. (IBIS), (2017) *"Summary of Wildlife Strikes Reported To the Icao Bird Strike Information System (Ibis) for the Years 2008 - 2015"* **Antimicrobial agents and chemotherapy *58***: 7250–7.

[4] M. S. Tatlıer and T. Baran, (2020) *"Structural and CFD analysis of an airfoil subjected to bird strike"* **European Journal of Mechanics, B/Fluids *84***: 478–486. DOI: 10.1016/j.euromechflu.2020.07.012.

[5] I. C. Metz, J. Ellerbroek, T. Mühlhausen, D. Kügler, and J. M. Hoekstra, (2020) *"The bird strike challenge"* **Aerospace *7***: 1–20. DOI: 10.3390/aerospace7030026.

[6] A. F. El-Sayed. *Bird strike in aviation : statistics, analysis and management*. Ed. by A. F. El-Sayed. first. John Wiley & Sons Ltd, 2019. DOI: 10.1002/9781119529835.

[7] B. Yadav, (2017) *"Aircraft Collisions and Bird Strikes in Nepal Between 1946-2016: A Case Study"* **Journal of Aeronautics & Aerospace Engineering *06***: DOI: 10.4172/2168-9792.1000203.

[8] J. Juračka, J. Chlebek, and V. Hodaň, (2022) *"Bird strike as a threat to aviation safety"* **Transportation Research Procedia *59***: 281–291. DOI: 10.1016/j.trpro.2021.11.120.

[9] A. Riccio, R. Cristiano, S. Saputo, and A. Sellitto, (2018) *"Numerical methodologies for simulating bird-strike on composite wings"* **Composite Structures *202***: 590–602. DOI: 10.1016/j.compstruct.2018.03.018.

[10] J. Liu, Y. Li, X. Yu, Z. Tang, X. Gao, J. Lv, and Z. Zhang, (2017) *"A novel design for reinforcing the aircraft tail leading edge structure against bird strike"* **International Journal of Impact Engineering *105***: 89–101. DOI: 10.1016/j.ijimpeng.2016.12.017.

[11] S. Long, X. Mu, Y. Liu, H. Wang, X. Zhang, and X. Yao, (2021) *"Failure modeling of composite wing leading edge under bird strike"* **Composite Structures *255***: 113005. DOI: 10.1016/j.compstruct.2020.113005.

[12] M. May, S. Arnold-Keifer, V. Landersheim, D. Laveuve, C. C. Asins, and M. Imbert, (2021) *"Bird strike resistance of a CFRP morphing leading edge"* **Composites Part C: Open Access *4***: DOI: 10.1016/j.jcomc.2021.100115.

[13] M. S. TATLIER, (2020) *"A Numerical Investigation of a Bird Strike on the Structure of an Aircraft Wing Leading Edge"* **European Mechanical Science *4***: 37–40. DOI: 10.26701/ems.622830.

[14] Y. Wang, X. Zheng, R. Hu, and P. Wang, (2016) *"Effects of leading edge defect on the aerodynamic and flow characteristics of an s809 Airfoil"* **PLoS ONE *11***: 1–17. DOI: 10.1371/journal.pone.0163443.

[15] S. P. Venkatesan, V. P. Kumar, M. S. Kumar, and S. Kumar, (2018) *"Computational analysis of aerodynamic characteristics of dimple airfoil NACA 2412 at various angles of attack"* **International Journal of Mechanical Engineering and Technology *9***: 41–49.

[16] D. A. Kumar and V. Girija, (2018) *"A Review on Bird-Strike Analysis on Leading Edge of an Aircraft Wing Structure using a SPH Formulation"*: 330–334.

[17] S. S. Rajan, M. Santhoshkumar, N. Lakshmanan, S. N. Pillai, and M. Paramasivam, (2009) *"CFD analysis and wind tunnel experiment on a typical launch vehicle model"* **Tamkang Journal of Science and Engineering *12***: 223–229.

[18] W. M. Elnaggar, Z. H. Chen, and Z. G. Huang, (2016) *"Numerical investigations of body tail projectile"* **Journal of Applied Science and Engineering *19***: 163–168. DOI: 10.6180/jase.2016.19.2.06.

[19] J. S. Lin, C. H. Chang, and N. C. Shang, (2006) *"Computational simulation and comparison of the effect of different surroundings on wind loads on domed structures"* **Tamkang Journal of Science and Engineering *9***: 291–297.

[20] S. M. Zakir and Y. Li, (2012) *"Dynamic response of the leading edge wing under soft body impact"* **International Journal of Crashworthiness *17***: 357–376. DOI: 10.1080/13588265.2012.661239.

[21] L. E. Stone, P. W. Wypych, D. B. Hastie, and S. Zigan, (2016) *"CFD-DEM modelling of powder flows and dust generation mechanisms - A review"* **ICBMH 2016 - 12th International Conference on Bulk Materials Storage, Handling and Transportation, Proceedings**: 417–426.

[22] Y. Wang, R. Hu, and X. Zheng, (2017) *"Aerodynamic Analysis of an Airfoil With Leading Edge Pitting Erosion"* **Journal of Solar Energy Engineering, Transactions of the ASME *139***: 1–11. DOI: 10.1115/1.4037380.

[23] D. W. A. Perdana and M. Effendy, (2021) *"Studi Numerik dan Eksperimen Aerodinamika Airfoil NACA 24112"* **Creative Research in Engineering *1***: 1. DOI: 10.30595/cerie.v1i1.9194.

[24] Z. Wu, Z. Xie, P. Wang, and W. Ding, (2020) *"Aerodynamic drag performance analysis of different types of high-speed train pantograph fairing"* **Journal of Applied Science and Engineering *23***: 509–519. DOI: 10.6180/jase.202009_23(3).0015.

[25] F. R. Menter, M. Kuntz, and R. Langtry, (2003) *"Ten Years of Industrial Experience with the SST Turbulence Model Turbulence heat and mass transfer"* **Cfd.Spbstu.Ru *4***: 625–632.